Contents

1 Interference Nulling Using Reconfigurable Intelligent Surface 1

1.1 Introduction 1

1.2 System Model 4

1.3 Interference Nulling via RIS 6

1.3.1 Feasibility of Interference Nulling 7

1.3.2 Alternating Projection Algorithm 12

1.3.3 Simulation Results 15

1.4 Learning to Minimize Interference 19

1.4.1 Learning to Initialize 22

1.4.2 Simulation Results 24

1.5 Conclusions 27

Bibliography 27

Chapter 1

Interference Nulling Using Reconfigurable Intelligent Surface

Tao Jiang,[1] Foad Sohrabi,[2] and Wei Yu[1*]

[1] *The Edward S. Rogers Sr. Department of Electrical and Computer Engineering, University of Toronto, M5S 3G4, Ontario, Toronto, Canada*
[2] *Nokia Bell Labs, NJ 07974, New Jersey, Murray Hill, USA*

*Corresponding Author: Wei Yu; weiyu@ece.utoronto.ca

1.1. Introduction

Reconfigurable intelligent surface (RIS) is a class of emerging devices [Di Renzo et al., 2019, Wu et al., 2021] that are capable of intelligently reconfiguring the wireless propagation channel by altering the phases of the reflected radio signals in a controlled manner. The RIS is typically made of many passive reconfigurable elements. It has very low energy consumption and can be easily integrated into the existing wireless communication systems. It provides a low-cost way of adaptively re-engineering the radio propagation channel and is envisioned as a key technology for the next generation wireless communication networks.

Most of the literature, e.g., [Huang et al., 2019, Wu and Zhang, 2019], have investigated the passive beamforming capability of the RIS. The idea is to reconfigure the passive elements of the RIS so that the incoming electromagnetic radiation is refocused with a narrow beam toward the intended receiver so that the signal-to-noise ratio (SNR) of the overall communication link is improved.

This chapter presents a new potential use of the RIS for a wireless environment with multiple transmitter-receiver pairs. The idea is to reconfigure the passive elements of the RIS so that the interferences between these multiple links can be reduced or even eliminated. In other words, the RIS is used to re-engineer a multiuser wireless communication channel so that all the links become effectively interference-free.

Consider a scenario in which K single-antenna transceiver pairs communicate independently while utilizing the same set of time and frequency resources. When the transmitters and the receivers are located close to each other, the interferences between these independent transmissions are typically the main channel impairments. The main insight of this chapter is that as long as the direct channels between the transmitters and the receivers are not too strong as compared to the reflected path through the RIS, it is possible to reconfigure the RIS in such a way that the interferences are completely eliminated in the overall effective channels. This is possible if the RIS has a sufficiently large number of elements — in the order of $O(K^2)$.

In conventional wireless communication deployment scenarios, interference is managed by scheduling nearby transmit-receive links into different time or frequency resource blocks. This leads to traditional deployment strategies such as frequency reuse but is not the most spectrally efficient. Modern wireless systems are often designed with full frequency reuse. To deal with interference,

modern wireless systems utilize spatial domain techniques based on multiple-input multiple-output (MIMO) technology (e.g., zero-forcing beamforming) to spatially separate the communication links. The main result of this chapter is that instead of relying on multiple antennas either at the transmitter or at the receiver to separate the interfering transmission pairs, it is possible to use a sufficiently large intelligent reflector to modify the $K \times K$ wireless channel so that it becomes interference-free, even for the case in which all the transmitters and the receivers are equipped with a single antenna only.

From a theoretical perspective, it is possible to show that under a rectangular array model of RIS, if the number of elements is sufficiently large and if the direct channels between the transceivers are blocked and the reflection channels between the transceivers and the RIS have line-of-sight, then it is always possible to tune the phase shifts of the RIS so that the effective overall channel is interference-free. From an algorithmic perspective, when the channel state information (CSI) is fully available, it is possible to use an alternating projection algorithm to efficiently find an interference-nulling solution numerically. Such an algorithm can be used either with or without the direct channels between the transceivers being present. Numerical results show that the alternating projection algorithm can find an interference-nulling solution if the number of RIS elements is slightly greater than $2K(K-1)$ and the direct links are weak.

The above results rely on the availability of perfect CSI. However, obtaining an accurate estimate of the CSI in an RIS system would in general require the number of pilots to scale with $O(KN)$, where N is the number of RIS elements. This is a huge overhead, because N is typically large. Poor channel estimation can lead to a solution with high interference power. The

second part of the chapter describes a learning-based method for finding the RIS configuration that can be easily incorporated into the conventional channel estimation and optimization framework with much reduced pilot training overhead. Specifically, using a few received pilots, the scheme first uses a linear minimum mean square estimator (LMMSE) to estimate the channel, then utilizes a deep neural network (DNN) to learn an initial point for the alternating projection algorithm from the estimated channel. This proposed method is based on the observation that the RIS optimization problem is highly nonconvex and different initial points can lead to solutions with different interference power. As compared to the conventional methods using random initial points for the alternating projection algorithm, simulations show that a DNN can learn a better initial point that can lead to a solution with significantly lower interference power at the same pilot length.

The interference cancelation capability of RIS has been investigated for device-to-device (D2D) communications in the cellular network [Fu et al., 2021, Chen et al., 2021, Ji et al., 2022, Abrardo et al., 2021]. In that setting, the RIS is used to mitigate interference from the D2D communications to the cellular communications. Most existing works also assume that perfect CSI is available when designing the reflection coefficients. This chapter studies the interference-nulling capability of RIS in a K-user interference channel and explicitly studies the impact of imperfect CSI.

1.2. System Model

Consider an RIS-assisted K-user interference environment, in which K single-antenna transceiver pairs communicate simultaneously using the same fre-

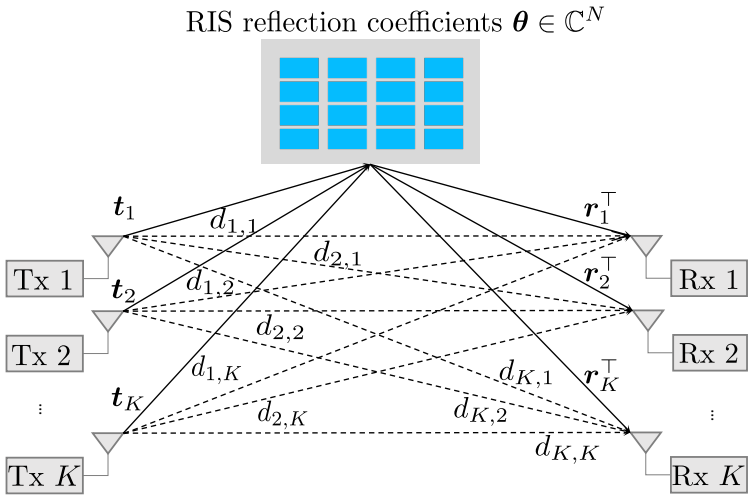

Figure 1.1: System model of RIS-assisted K-user interference environment.

quency and time resources. As shown in Figure 1.1, an RIS is deployed between the transmitters and receivers. The idea is to tune the phase shifts of the RIS to create an interference-free communication network. We assume a block fading channel model where the channels remain constant in one coherence block but change independently across different coherence blocks. Let $\boldsymbol{t}_j \in \mathbb{C}^N$ denote the channel from the j-th transmitter to the RIS, and $\boldsymbol{r}_k^\top \in \mathbb{C}^{1\times N}$ denote the channel from the RIS to the k-th receiver. The RIS is modeled as an array of phase shifters. Let $\omega_i \in (0, 2\pi]$ be the phase shift of the i-th element of the RIS, then the reflection coefficients of the RIS can be denoted by $\boldsymbol{\theta} = [e^{j\omega_1}, \ldots, e^{j\omega_N}]^\top \in \mathbb{C}^N$. The direct channel from the j-th transmitter to the k-th receiver without the RIS reflection is denoted as $d_{k,j} \in \mathbb{C}$. The received signal at the k-th receiver can be represented as

$$y_k = \sum_{j=1}^{K} \left(\boldsymbol{r}_k^\top \operatorname{diag}(\boldsymbol{\theta}) \boldsymbol{t}_j + d_{k,j} \right) x_j + n_k, \tag{1.1}$$

where $x_j \in \mathbb{C}$ is the transmitted signal from the j-th transmitter and intended to the j-th receiver, and $n_k \sim \mathcal{CN}(0, \sigma^2)$ is the additive Gaussian noise. The transmitted signal is subject to a power constraint, i.e., $\mathbb{E}\left[|x_j|^2\right] = p_j$, where p_j is the transmit power of the j-th transmitter.

With these notations, the theoretical achievable rate of the k-th transceiver pair can now be written as

$$R_k = \log_2\left(1 + \frac{p_k|\boldsymbol{r}_k^\top \operatorname{diag}(\boldsymbol{\theta})\boldsymbol{t}_k + d_{k,k}|^2}{\sum_{j\neq k} p_j|\boldsymbol{r}_k^\top \operatorname{diag}(\boldsymbol{\theta})\boldsymbol{t}_j + d_{k,j}|^2 + \sigma^2}\right). \tag{1.2}$$

The chapter focuses on designing the reflection coefficients $\boldsymbol{\theta}$ to create K interference-free channels for the corresponding K transceiver pairs. This achieves the maximum degrees-of-freedom K for the system.

1.3. Interference Nulling via RIS

To achieve the maximum degrees-of-freedom of the overall K-user system, we need to find a configuration of the RIS reflection coefficients $\boldsymbol{\theta}$ such that all the interference is nulled and the desired links have positive effective channel strength, i.e.,

$$\boldsymbol{r}_k^\top \operatorname{diag}(\boldsymbol{\theta})\boldsymbol{t}_j + d_{k,j} = 0, \quad \forall j \neq k,\ \forall k = 1, \ldots, K, \tag{1.3a}$$

$$\boldsymbol{r}_k^\top \operatorname{diag}(\boldsymbol{\theta})\boldsymbol{t}_k + d_{k,k} \neq 0, \quad \forall k = 1, \ldots, K. \tag{1.3b}$$

Let $\boldsymbol{a}_{k,j} \triangleq \text{diag}(\boldsymbol{t}_j)\boldsymbol{r}_k$ denote the cascaded channel from transmitter j to receiver k, the conditions in (1.3) can be rewritten in the following form:

$$\boldsymbol{a}_{k,j}^{\top}\boldsymbol{\theta} + d_{k,j} = 0, \quad \forall j \neq k, \ \forall k = 1, 2, \ldots, K, \tag{1.4a}$$

$$\boldsymbol{a}_{k,j}^{\top}\boldsymbol{\theta} + d_{k,k} \neq 0, \quad \forall k = 1, 2, \ldots, K. \tag{1.4b}$$

Since the channel realizations are random, the conditions in (1.4b) hold almost surely. Thus, we focus on seeking a feasible solution $\boldsymbol{\theta}$ to the conditions in (1.4a). Note that the RIS coefficients are subject to the constraint $\boldsymbol{\theta} = [e^{j\omega_1}, \ldots, e^{j\omega_N}]$, so finding a feasible set of phase shifts $\{\omega_1, \ldots, \omega_N\}$ is a highly nontrivial problem.

1.3.1. Feasibility of Interference Nulling

The conditions in (1.4a) are not always feasible. If the RIS reflection coefficients are treated as unconstrained variables, the number of complex variables N should be greater than the number of complex linear equations $K(K-1)$ to guarantee that the set of equations (1.4a) has a solution. This would be the case if both the amplitude and phase can be controlled arbitrarily for each RIS element. If only the phase of the RIS can be configured, that is, the RIS coefficient vector is subject to the constraint $\boldsymbol{\theta} = [e^{j\omega_1}, \ldots, e^{j\omega_N}]$, the feasibility problem becomes more complicated. By simply counting the number of equations and the number of variables in the real field, we can see that there are N real variables ω_i in $\boldsymbol{\theta}$ and $2K(K-1)$ nonlinear real equations of ω_i's in (1.4a). Therefore, intuitively we would need $N \geq 2K(K-1)$ to ensure that there exists a feasible solution to (1.4a).

However, it is not easy to establish the above results rigorously since the

equations of the phase shifts ω_i's are nonlinear. Further, even if the existence of the interference-nulling solutions can be guaranteed, finding a solution is still computationally challenging. Nevertheless, later in this chapter, we show that the intuition of requiring $N \geq 2K(K-1)$ is correct and present a computationally efficient alternating projection algorithm, which can be used to find an interference nulling solution when N is slightly larger than $2K(K-1)$. Before going into the algorithm, we first present a theoretical result that provides a sufficient condition for the feasibility of (1.4a) for a specific RIS model and specific deployment scenario. This theoretical result suggests that for an RIS-assisted network with negligible direct channels and line-of-sight transceiver-RIS channels, the interference can be completely nulled out by a uniform rectangular RIS with a sufficiently large number of reflective elements.

Specifically, consider an $N_1 \times N_2$ uniform rectangular array RIS, which has N_1 elements per row (horizontal direction) and N_2 elements per column (vertical direction). Denote $\varrho \in [-\frac{\pi}{2}, \frac{\pi}{2}]$, $\phi \in [-\frac{\pi}{2}, \frac{\pi}{2}]$ as the azimuth angle and the elevation angle of arrival, respectively. We can write the n-th element of the RIS steering vector as follows [Björnson and Sanguinetti, 2021]:

$$[\boldsymbol{\psi}(\varrho, \phi)]_n = e^{j\frac{2\pi}{\lambda}[i_1(n)b_1 \sin(\varrho)\cos(\phi) + i_2(n)b_2 \sin(\phi)]}, \tag{1.5}$$

where b_1 and b_2 are the horizontal and vertical spacings between the RIS elements, and $i_1(n) = \mathrm{mod}(n-1, N_1)$ and $i_2(n) = \lfloor (n-1)/N_2 \rfloor$ denote the horizontal index and vertical index of element n, respectively. The channel vector between the RIS and the k-th transmitter can then be written as

$$\boldsymbol{t}_k = \beta_k^{\mathrm{t}} \boldsymbol{\psi}(\varrho_k^{\mathrm{t}}, \phi_k^{\mathrm{t}}), \tag{1.6}$$

where β_k^{t} denotes the pathloss between the k-th transmitter and the RIS, and ϱ_k^{t} and ϕ_k^{t} are the corresponding azimuth and elevation angles. Similarly, we represent the channel between RIS and the k-th receiver as $\boldsymbol{r}_k = \beta_k^{\mathrm{r}} \boldsymbol{\psi}(\varrho_k^{\mathrm{r}}, \phi_k^{\mathrm{r}})$.

When the direct channels can be ignored, the interference nulling conditions (1.4) become

$$\boldsymbol{a}_{k,j}^{\top} \boldsymbol{\theta} = 0, \quad \forall j \neq k, \ \forall k = 1, 2, \ldots, K. \tag{1.7a}$$

$$\boldsymbol{a}_{k,j}^{\top} \boldsymbol{\theta} \neq 0, \quad \forall k = 1, 2, \ldots, K, \tag{1.7b}$$

where $\boldsymbol{\theta} = [e^{j\omega_1}, \ldots, e^{j\omega_N}]$. In order to find a sufficient condition for the feasibility of (1.7), we use the following lemma, which ensures the existence of a polynomial with unit modulus coefficients for given roots on the complex unit circle.

Lemma 1.1 ***(Newman and Giroux [1990])*:** *Given $z_1, \ldots, z_n$ on the complex unit circle $\mathcal{C} = \{x \in \mathbb{C} : |x| = 1\}$, there exists a polynomial f of degree $\sum_{i=1}^{n} 4^{i-1}$ with unit modulus coefficients such that the points $z_1, \ldots, z_n$ are the only zeros of f on $\mathcal{C}$.*

Now, we establish the following sufficient condition for the feasibility of the interference nulling criterion (1.7).

Theorem 1.1: *For an $N_1 \times N_2$ rectangular RIS, assuming that the channels between the RIS and the users are given by* (1.6)*, there exists a feasible solution to the interference nulling conditions in* (1.7) *if either $N_1 = \sum_{k=1}^{K(K-1)} 4^{k-1}$ or $N_2 = \sum_{k=1}^{K(K-1)} 4^{k-1}$.*

Proof. We begin with the case $N_2 = 1$, which corresponds to the uniform

linear array case. In this case, the channel between the RIS and transmitter j can be written as

$$\boldsymbol{t}_j = \beta_j^{\mathrm{t}}[1, \ldots, e^{j\frac{2\pi b_2(N_1-1)}{\lambda}\sin(\phi_j^{\mathrm{t}})}]^\top, \tag{1.8}$$

and the channel between the RIS and receiver k can be written as

$$\boldsymbol{r}_k = \beta_k^{\mathrm{r}}[1, \ldots, e^{j\frac{2\pi b_2(N_1-1)}{\lambda}\sin(\phi_k^{\mathrm{r}})}]^\top. \tag{1.9}$$

Thus, we have

$$\boldsymbol{a}_{k,j} = \beta_k^{\mathrm{r}}\beta_j^{\mathrm{t}}[1, \ldots, e^{j\frac{2\pi b_2(N_1-1)}{\lambda}(\sin(\phi_j^{\mathrm{t}})+\sin(\phi_k^{\mathrm{r}}))}]^\top \tag{1.10a}$$

$$\triangleq \beta_k^{\mathrm{r}}\beta_j^{\mathrm{t}}[1, z_{k,j}, z_{k,j}^2, \ldots, z_{k,j}^{N_1-1}]^\top, \tag{1.10b}$$

where $z_{k,j} = e^{j\frac{2\pi b_2}{\lambda}(\sin(\phi_j^{\mathrm{t}})+\sin(\phi_k^{\mathrm{r}}))}$.

Let $f(z)$ denote a polynomial of degree N_1 with unit modulus coefficients as follows:

$$f(z) = \theta_1 + \theta_2 z + \theta_3 z^2 + \ldots + \theta_{N_1} z^{N_1-1}, \tag{1.11}$$

where $|\theta_i| = 1,\ \forall i$. Observe that the interference nulling conditions in (1.7a) and (1.7b) can now be expressed as below with the coefficients of $f(z)$ playing the role of RIS phase shifts:

$$f(z_{k,k}) \neq 0, \quad k = 1, \ldots, K, \tag{1.12a}$$

$$f(z_{k,j}) = 0, \quad k = 1, \ldots, K, \ \ \forall j \neq k. \tag{1.12b}$$

Thus, the original problem of finding RIS phase shifts for interference nulling is

now transformed into the problem of finding a polynomial with unit modulus coefficients as in (1.11) such that $z_{k,j}$'s are the roots, while the polynomial does not vanish at $z_{k,k}$'s. By Lemma 1.1, we know such a polynomial exists if $N_1 = \sum_{k=1}^{K(K-1)} 4^{k-1}$.

To generalize the above result to the rectangular array case with $N_2 > 1$, we make the argument that a rectangular uniform array can be viewed as N_2 rows of the uniform linear array of size $N_1 \times 1$. Thus, if we set all the rows of the RIS to have the same reflection coefficients that null all the interference, which can be achieved if $N_1 = \sum_{k=1}^{K(K-1)} 4^{k-1}$, the entire rectangular array would also achieve the interference nulling condition. Mathematically, this means that the same reflection coefficients are used N_2 times to produce a zero-forcing solution for all N_2 sub-vectors of $\boldsymbol{\psi}(\varrho, \phi)$ as in (1.5).

Finally, if we exchange the roles of N_1 and N_2, it is easily seen that the interference nulling conditions are also achievable if $N_2 = \sum_{k=1}^{K(K-1)} 4^{k-1}$. This completes the proof.

Theorem 1.1 is a theoretical result showing that an interference nulling solution must exist if the number of RIS elements N scales as the exponential function of K. But in practice, we empirically find that by using an alternating projection algorithm, a feasible solution can be found as long as the number of RIS elements N is only slightly larger than the number of nonlinear equations $2K(K-1)$.

We remark that if the direct channel $d_{k,j}$ is present, the feasibility condition becomes more strict since it is necessary to have

$$\|\boldsymbol{a}_{k,j}\|_1 \geq |d_{k,j}|, \quad \forall k = 1, \ldots, K, \ j \neq k, \tag{1.13}$$

as otherwise even aligning all the strength of the cascaded channel would not

be sufficient to cancel out the interference in the direct channel $d_{k,j}$. It can be observed that as the strength of the direct channel increases, the number of RIS elements N also needs to increase in order to make interference nulling feasible.

1.3.2. Alternating Projection Algorithm

This section presents an alternating projection algorithm for finding an interference nulling solution to (1.4). The proposed algorithm is applicable regardless of the RIS channel model and regardless of whether the direct links are present.

Specifically, we formulate the problem of finding an interference-nulling solution as the following feasibility problem:

$$\begin{aligned} \text{find} \quad & \boldsymbol{\theta} && \text{(1.14a)} \\ \text{subject to} \quad & \boldsymbol{a}_{k,j}^{\top}\boldsymbol{\theta} + d_{k,j} = 0, \quad k = 1, \ldots, K, \ \forall j \neq k, && \text{(1.14b)} \\ & |\theta_i| = 1, \quad i = 1, \ldots, N. && \text{(1.14c)} \end{aligned}$$

For ease of presentation, let $\boldsymbol{A}_k \in \mathbb{C}^{N \times (K-1)}$ denote the collection of all the interference channels to the k-th receiver through the reflection of the RIS, i.e.,

$$\boldsymbol{A}_k = [\boldsymbol{a}_{k,1}, \ldots, \boldsymbol{a}_{k,k-1}, \boldsymbol{a}_{k,k+1}, \ldots, \boldsymbol{a}_{k,K}]. \tag{1.15}$$

Let $\boldsymbol{d}_k \in \mathbb{C}^{K-1}$ denote all the interference channels to the k-th receiver through the direct links, i.e.,

$$\boldsymbol{d}_k = [d_{k,1}, \ldots, d_{k,k-1}, d_{k,k+1}, \ldots, d_{k,K}]^{\top}. \tag{1.16}$$

To further simplify the notation, let

$$\boldsymbol{A} = [\boldsymbol{A}_1, \ldots, \boldsymbol{A}_K], \tag{1.17a}$$

$$\boldsymbol{d} = [\boldsymbol{d}_1^\top, \ldots, \boldsymbol{d}_K^\top]^\top, \tag{1.17b}$$

where $\boldsymbol{A} \in \mathbb{C}^{N\times(K-1)K}$ and $\boldsymbol{d} \in \mathbb{C}^{(K-1)K}$ contain all the interference channels through the RIS reflection and the direct link, respectively.

Then, (1.14) can be rewritten more compactly as

$$\begin{aligned} \text{find} \quad & \boldsymbol{\theta} && \text{(1.18a)} \\ \text{subject to} \quad & \boldsymbol{A}^\top\boldsymbol{\theta} + \boldsymbol{d} = \boldsymbol{0}, && \text{(1.18b)} \\ & |\theta_i| = 1, \quad i = 1, \ldots, N. && \text{(1.18c)} \end{aligned}$$

Problem (1.18) is computationally challenging to solve due to the nonconvex unit modulus constraints.

To solve this problem efficiently, this chapter presents an alternating projection algorithm that transforms the feasibility problem (1.18) into a problem of finding a point in the intersection of two sets. For ease of presentation, we define the following two constraint sets

$$\mathcal{S}_1 = \{\boldsymbol{\theta} : \boldsymbol{A}^\top\boldsymbol{\theta} + \boldsymbol{d} = \boldsymbol{0}\}, \tag{1.19a}$$

$$\mathcal{S}_2 = \{\boldsymbol{\theta} : |\theta_i| = 1,\ i = 1, \ldots, N\}, \tag{1.19b}$$

and rewrite problem (1.18) equivalently as

$$\begin{aligned} \text{find} \quad & \boldsymbol{\theta} \\ \text{subject to} \quad & \boldsymbol{\theta} \in \mathcal{S}_1 \cap \mathcal{S}_2. \end{aligned} \tag{1.20}$$

The feasibility problem (1.18) now becomes that of finding a point in the intersection of $\mathcal{S}_1$ and $\mathcal{S}_2$. To this end, given an initial point $\boldsymbol{\theta}^{(0)}$, the alternating projection algorithm alternatively projects onto $\mathcal{S}_1$ and $\mathcal{S}_2$ as follows:

$$\tilde{\boldsymbol{\theta}}^{(t)} = \Pi_{\mathcal{S}_1}(\boldsymbol{\theta}^{(t)}), \tag{1.21a}$$

$$\boldsymbol{\theta}^{(t+1)} = \Pi_{\mathcal{S}_2}(\tilde{\boldsymbol{\theta}}^{(t)}), \tag{1.21b}$$

where the operator $\Pi_{\mathcal{S}}(\boldsymbol{\theta})$ denotes the Euclidean projection of $\boldsymbol{\theta}$ onto $\mathcal{S}$, defined as the solution to the following problem:

$$\begin{aligned} \underset{\boldsymbol{x}}{\text{minimize}} \quad & \|\boldsymbol{\theta} - \boldsymbol{x}\|_2^2 \\ \text{subject to} \quad & \boldsymbol{x} \in \mathcal{S}. \end{aligned} \tag{1.22}$$

Fortunately, the projections onto the sets $\mathcal{S}_1$ and $\mathcal{S}_2$ both have simple analytical expressions, as given by [Parikh and Boyd, 2014]:

$$\Pi_{\mathcal{S}_1}(\boldsymbol{\theta}) = \boldsymbol{\theta} - \boldsymbol{A}^*(\boldsymbol{A}^\top \boldsymbol{A}^*)^{-1}(\boldsymbol{A}^\top \boldsymbol{\theta} + \boldsymbol{d}), \tag{1.23a}$$

$$\Pi_{\mathcal{S}_2}(\boldsymbol{\theta}) = \boldsymbol{\theta}/|\boldsymbol{\theta}|, \tag{1.23b}$$

where $\boldsymbol{A}^*$ is complex conjugate of $\boldsymbol{A}$. In (1.23a) the channel matrix $\boldsymbol{A}$ is assumed to be full column rank (otherwise the matrix $\boldsymbol{A}$ can be replaced by a new matrix $\boldsymbol{A}'$ constructed from the basis of the column space of $\boldsymbol{A}$). In (1.23b), if some elements of the vector $\boldsymbol{\theta}$ are zero, these elements can be projected to any random point on the complex unit circle. The alternating projection algorithm for solving problem (1.20) is summarized in Algorithm 1.

The local convergence of the alternating projection algorithm is established in [Jiang and Yu, 2022]. That is, if the intersection of the sets $\mathcal{S}_1$ and $\mathcal{S}_2$ is

Algorithm 1: Alternating Projection for Solving (1.18)

Input: Initial point $\boldsymbol{\theta} \in \mathbb{C}^N$. Channel matrix $\boldsymbol{A}$.
Initialization: $\boldsymbol{\theta}^{(0)} = \boldsymbol{\theta}$
for $t = 0, 1, 2, \ldots$ **do**
  $\tilde{\boldsymbol{\theta}}^{(t)} = \Pi_{\mathcal{S}_1}(\boldsymbol{\theta}^{(t)})$
  $\boldsymbol{\theta}^{(t+1)} = \Pi_{\mathcal{S}_2}(\tilde{\boldsymbol{\theta}}^{(t)})$
  if *stopping criterion is satisfied* **then**
    break
  end
end
Output: $\boldsymbol{\theta}^{(t+1)}$

nonempty, Algorithm 1 is guaranteed to converge to an intersection point of $\mathcal{S}_1$ and $\mathcal{S}_2$ from an initial point sufficiently close to the intersection point.

The computational complexity of the proposed algorithm is dominated by the step (1.23a). This step requires time complexity $O(N^2K^2 + K^6 + K^4N)$ for computing $\boldsymbol{A}^*(\boldsymbol{A}^\top \boldsymbol{A}^*)^{-1}\boldsymbol{A}^\top$. But, this matrix can be precalculated and reused in each iteration, so the overall time complexity of the Algorithm 1 is $O(N^2K^2 + K^6 + K^4N + tN^2)$, where t is the number of iterations required for convergence.

1.3.3. Simulation Results

To illustrate the performance of the proposed algorithm, we report the simulation results in [Jiang and Yu, 2022]. The results in Figure 1.2 and Figure 1.3 correspond to the scenario without direct links and the results in Figure 1.4 and Figure 1.5 correspond to the scenario with direct links.

In the simulations, an interference nulling solution is said to be found if the maximum interference-to-signal ratio across all transceiver pairs is below -36dB. In Figure 1.2, we plot the empirical probability of finding an interfer-

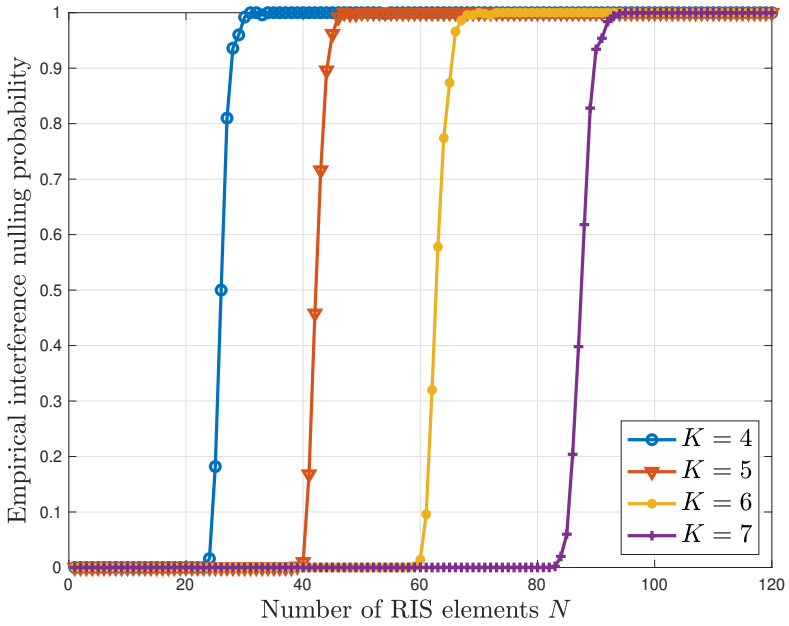

Figure 1.2: Empirical interference nulling probability vs. number of RIS elements in the scenario without direct links.

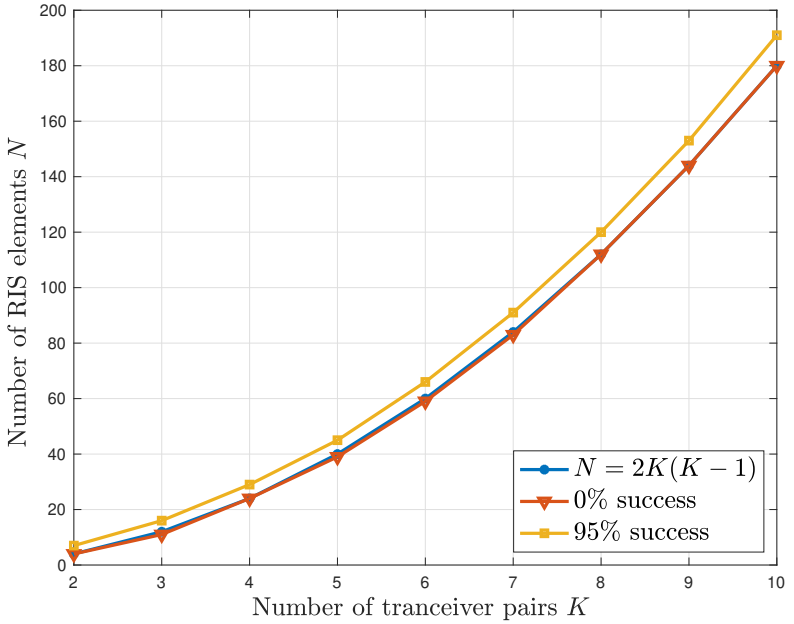

Figure 1.3: Number of RIS elements vs. number of transceiver pairs K in the scenario without direct links.

ence nulling solution for different numbers of RIS elements N and transceiver pairs K. It can be seen from Fig 1.2 that there is a phase transition phenomenon as N increases for each fixed K. The interference nulling probability is almost 0 if N is smaller than some threshold, while the probability increases to 1 dramatically if N exceeds the threshold. The threshold that the phase transition occurs is about $2K(K-1)$ as K varies.

To observe the phase transition location more precisely, Figure 1.3 shows the value of N below which there is a "0% success" rate for finding an interference-nulling solution and the points above which there is empirically a "95% success" rate for finding an interference-nulling solution. We also plot the line $N = 2K(K-1)$, which precisely matches the "0% success" line. This implies that $N \geq 2K(K-1)$ is a necessary condition for the feasibility of interference nulling. Both Figure 1.2 and Figure 1.3 show that the proposed alternating projection algorithm can find an interference nulling solution with high probability if the number of RIS elements N is slightly above the threshold $2K(K-1)$. It is also observed in simulations that the phase transition location is not sensitive to the channel model.

We present the results of the case with direct links in Figure 1.4 and Figure 1.5. In Figure 1.4, the number of transceiver pairs $K = 7$. The path loss of the cascaded channels is about -122.6 dB. As the path loss of the direct link $\tilde{\beta}_{k,j}$ becomes stronger, the phase transition location shifts towards a larger N as shown in Figure 1.4. This implies that more RIS elements are needed to cancel out the interference in the direct link.

From (1.13), we know that the relative strength of the cascaded channels and the direct channels can affect the interference nulling probability. So in Figure 1.5, we plot the empirical interference nulling probability for $K = 8$

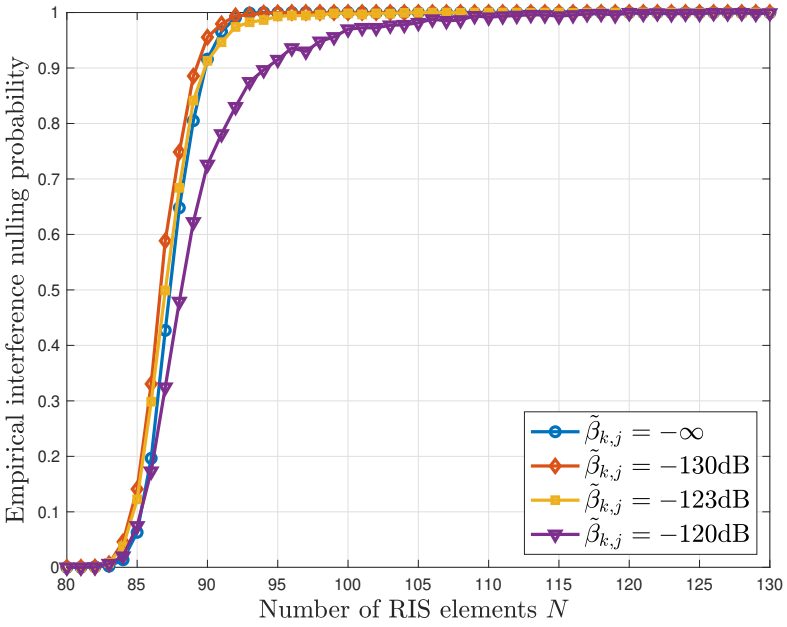

Figure 1.4: Empirical interference nulling probability vs. number of RIS elements in the scenario with direct links for a system with $K = 7$ transceiver pairs.

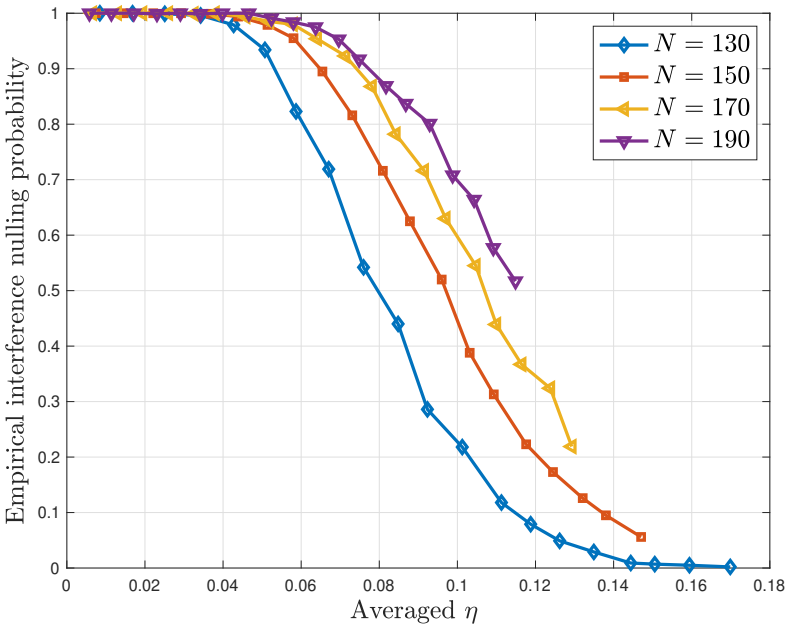

Figure 1.5: Empirical interference nulling probability vs. direct-to-reflective link strength η for a system with $K = 8$ transceiver pairs.

for various values of the ratio between the strength of the direct link and the cascaded channels, i.e.,

$$\eta = \max_{k,j} \frac{|d_{k,j}|}{\|\boldsymbol{a}_{k,j}\|_1}. \tag{1.24}$$

As can be seen from Figure 1.5, the empirical interference nulling probability decreases as the parameter η increases. To maintain high interference nulling probability as η increases, we need to increase the number of RIS elements.

1.4. Learning to Minimize Interference

The discussions so far in this chapter all assume that the perfect CSI is available for configuring the RIS. This represents the ultimate interference-nulling capability of the RIS system. But in practice the perfect CSI is never available; the CSI needs to be estimated using pilots with inherent channel estimation error. In this section, we consider the case where a pilot stage is used to obtain the CSI. We assume that the pilots are transmitted from the transmitter to the receiver and the received pilots are collected at a central node in order to design the reflection coefficients of the RIS. For simplicity, We ignore the direct links in this section but the proposed method can be readily extended to the scenario where the direct links exist.

We assume that the pilots are sent in a time orthogonal manner. Suppose that KL samples are reserved for the pilot stage in each coherence block. Each transmitter occupies L samples and sends a random sequence of L pilots while the other transmitters remain silent. More specifically, the j-th transmitter sends a sequence of pilots $x_j(1), \ldots, x_j(L)$, and the received pilots at the k-th

receiver are given by

$$y_{k,j}(\ell) = \boldsymbol{a}_{k,j}^{\top} \boldsymbol{\theta}(\ell) x_j(\ell) + n_{k,j}(\ell), \quad \ell = 1, \ldots, L, \tag{1.25}$$

where $\boldsymbol{\theta}(\ell)$ is the reflection coefficients in the ℓ-th pilot transmission slot (typically randomly chosen), $n_{k,j} \sim \mathcal{CN}(0, \sigma_2^2)$ is the additive noise and we set the pilot symbol $x_j(\ell) = 1$ without loss of generality.

Let $\boldsymbol{Y}_j \in \mathbb{C}^{K \times L}$ denote the matrix whose entry in the k-th row and ℓ-th column is $y_{k,j}(\ell)$, we have

$$\boldsymbol{Y}_j = \tilde{\boldsymbol{A}}_j^{\top} \boldsymbol{\Theta} + \boldsymbol{N}_j, \tag{1.26}$$

where $\tilde{\boldsymbol{A}}_j = [\boldsymbol{a}_{1,j}, \ldots, \boldsymbol{a}_{K,j}]$ contains the cascaded channel from transmitter j to all the K receivers and $\boldsymbol{\Theta} = [\boldsymbol{\theta}(1), \ldots, \boldsymbol{\theta}(L)]$. Concatenating $\boldsymbol{Y}_j$'s into a matrix $\boldsymbol{Y} = [\boldsymbol{Y}_1^{\top}, \ldots, \boldsymbol{Y}_K^{\top}]^{\top}$, we can write

$$\boldsymbol{Y} = \tilde{\boldsymbol{A}}^{\top} \boldsymbol{\Theta} + \boldsymbol{N}, \tag{1.27}$$

where $\tilde{\boldsymbol{A}} = [\tilde{\boldsymbol{A}}_1, \ldots, \tilde{\boldsymbol{A}}_K]$ and $\boldsymbol{N} = [\boldsymbol{N}_1^{\top}, \ldots, \boldsymbol{N}_K^{\top}]^{\top}$. Given the received pilots $\boldsymbol{Y}$ and the RIS reflection coefficients matrix $\boldsymbol{\Theta}$, a linear minimum mean square error (LMMSE) estimator for $\tilde{\boldsymbol{A}}$ takes the following form [Jiang et al., 2021]:

$$\begin{aligned} \hat{\boldsymbol{A}} = (\boldsymbol{Y} - \mathbb{E}[\boldsymbol{Y}])\, \mathbb{E}\left[(\boldsymbol{Y} - \mathbb{E}[\boldsymbol{Y}])^{\mathsf{H}} (\boldsymbol{Y} - \mathbb{E}[\boldsymbol{Y}]) \right]^{-1} \\ \mathbb{E}\left[(\boldsymbol{Y} - \mathbb{E}[\boldsymbol{Y}])^{\mathsf{H}} (\boldsymbol{A} - \mathbb{E}[\boldsymbol{A}]) \right] + \mathbb{E}[\boldsymbol{A}]. \end{aligned} \tag{1.28}$$

Using the estimated channel $\hat{\boldsymbol{A}}$, we can run the alternating projection algorithm (i.e., Algorithm 1) to obtain an interference nulling solution. The overall algorithmic framework is illustrated in Figure 1.6.

Obtaining a good interference nulling solution, however, requires a very accurate estimate of the channel, which in turn requires significant pilot overhead. If the estimated channel is not sufficiently accurate, the alternating projection algorithm often returns an interference-nulling solution that still results in a relatively high level of interference. This is because the alternating projection algorithm is very sensitive to the channel estimation error.

To reduce the pilots training overhead, it is possible to use machine-learning approaches to directly map the received pilots to the reflection coefficients [Özdoğan and Björnson, 2020, Jiang et al., 2021, Zhang et al., 2022, Sohrabi et al., 2022]. Through end-to-end learning, the neural network can be trained to exploit the received pilots more efficiently for optimizing the final task objective [Yu et al., early access, 2022]. However, applying such an idea to the considered interference-nulling problem is suitable only if the target interference power is not too close to zero. If the target interference power level is too low, an enormous amount of training data and a huge DNN would be required to obtain an accurate zero-forcing solution.

For the task of learning a highly accurate solution to an optimization problem, algorithm unfolding-based neural network architecture can often be used to achieve good performance with reasonably sized training sets [Monga et al., 2021, Chen et al., 2022]. In the algorithm unfolding-based DNN, each layer mimics an iteration of an particular algorithm with some parameters being made trainable. This ensures that the DNN is capable of achieving at least as good performance as the original algorithm and can potentially obtain performance gain by tuning the trainable parameters to make the algorithm tailored to the specific data distribution in the training stage.

In this section, we propose an unfolding-based DNN architecture to learn

the interference-nulling solution from received pilots. But the alternating projection algorithm described earlier in the chapter is actually parameter-free, so we propose to include trainable parameters *before* the alternating projection algorithm for producing the initial point (instead of having trainable parameters within each iteration). This is also justified by the fact that the considered optimization problem is highly nonconvex, so different initial points lead to solutions with different performances. The hope is that the DNN can learn a better initial point from the training instances of the problem than the traditional random initialization strategy.

1.4.1. Learning to Initialize

To reduce the pilot training overhead and make the algorithm robust in the imperfect CSI scenario, this chapter proposes a learning approach that can find a better interference-nulling solution than the conventional approach. This is achieved by using a neural network to learn a good initial point for the subsequent alternating projection algorithm.

The overall framework of the proposed learning method is illustrated in Figure 1.7. The central node first collects the received pilots in the pilot stage and uses an LMMSE layer described in (1.28) to extract an estimation of the interference channel matrix $\hat{\boldsymbol{A}}$. The matrix $\hat{\boldsymbol{A}}$ is used to form the alternating projection steps and as the input to the DNN initialization layer. The DNN initialization layer then outputs an initial point $\boldsymbol{\theta}^{(0)}$ as the input to the subsequent alternating projection algorithm, which consists of T layers. The neural network is trained end-to-end to minimize the loss function $-\mathbb{E}[\|\boldsymbol{A}^\top \boldsymbol{\theta}^{(T)}\|_2^2]$, where $\boldsymbol{\theta}^{(T)}$ is the solution after T layer iterations. In the training stage, the

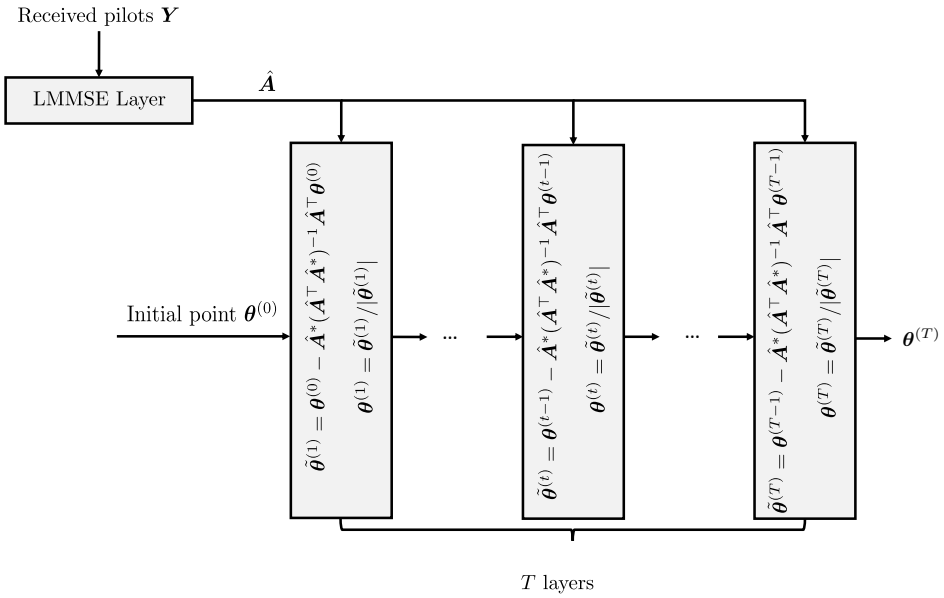

Figure 1.6: Conventional method runs the alternating projection algorithm from a random initial point.

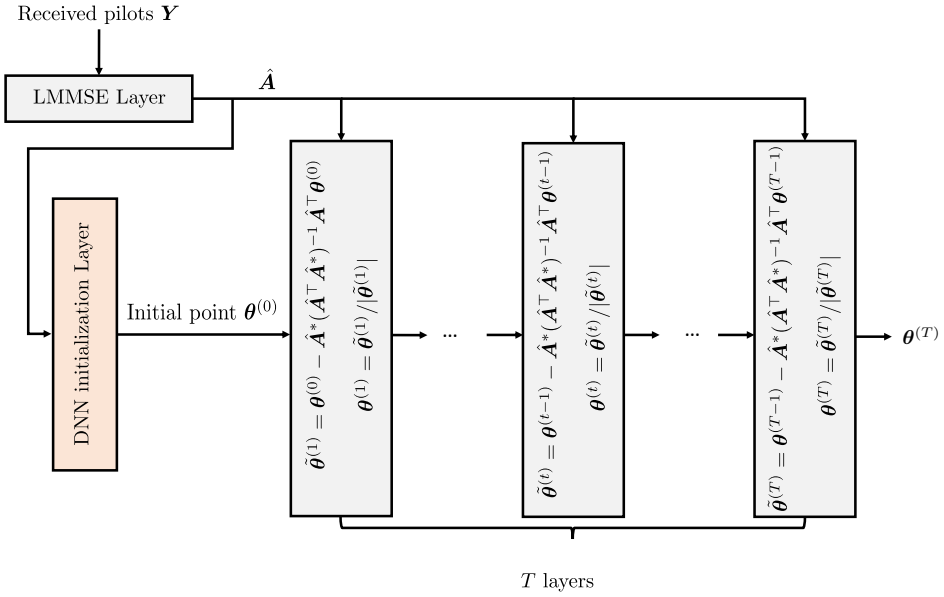

Figure 1.7: Proposed approach uses a deep neural network to learn a good initial point.

DNN aims to learn to produce an initial point that leads to a solution with lower interference power when evaluated on the true channel matrix $\boldsymbol{A}$.

As shown in Figure 1.7, the proposed learning-based method is quite similar to the conventional approach in Figure 1.6 except that an additional DNN layer outputs the initial points for the subsequently alternating projection algorithm. So the complexities of these two approaches are almost the same. In the following simulations, we can see that the DNN initialization layer can learn a more robust initial point than the conventional scheme with random initialization.

1.4.2. Simulation Results

To illustrate the performance of the proposed DNN, we use a simulation setting with the number of RIS elements $N = 64$ and the number of transceivers $K = 4$. The channels between the RIS and the transceivers are assumed to be multipath channels of the form $\boldsymbol{t} = \frac{1}{\sqrt{L_p}} \sum_{i=1}^{L_p} \alpha_i \boldsymbol{\psi}(\varrho_i, \phi_i)$, where $L_p = 3$ is the number of paths, $\alpha_i \sim \mathcal{CN}(0, 1)$ is the fading coefficient and $\boldsymbol{\psi}(\varrho_i, \phi_i)$ is the steering vector of RIS with azimuth and elevation angles of arrival (ϱ_i, ϕ_i). The SNR in the pilot stage is 25dB. The number of iterations of the alternating projection algorithm is 30.

In Figure 1.8, we compare the performance between the conventional channel estimation method followed by alternating projection (AP) with random initialization and the proposed method with DNN initialization. Assuming a transmit power of 23 dBm and a pathloss of -108 dB for all $K = 4$ links, the total interference power across the 4 users is plotted for the two cases. As can be seen from Figure 1.8, the interference powers of both methods decrease

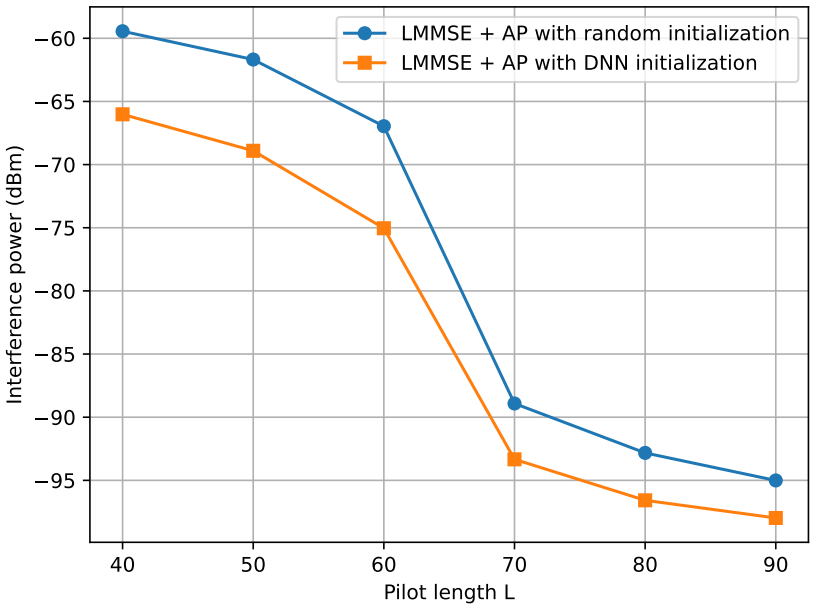

Figure 1.8: Performance comparison for a system with $N = 64$ RIS elements and $K = 4$ transceiver pairs.

as the pilot length L increases, but the proposed approach achieves a much lower interference level than the conventional method with random initialization. This implies that the neural network learns a better initial point for the downstream alternating projection algorithm.

To investigate where the performance gain comes from, we conduct a simulation where many random initial points are used to run the alternating projection algorithm based on the estimated interference channel $\hat{\boldsymbol{A}}$. The system setting is as follows, $N = 64$, $K = 4$, and $L = 70$. After the algorithm converges, we compute the interference power based on the true interference channel $\boldsymbol{A}$. We report the minimum total interference power across the solutions obtained from different initial points in Figure 1.9. It can be seen that as the number of random initial points increases, the total interference power for the alternat-

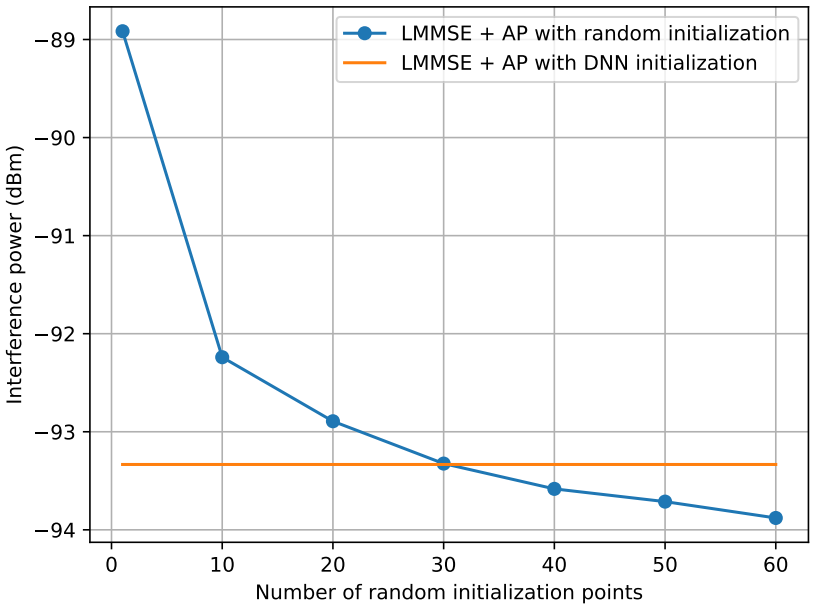

Figure 1.9: Performance comparison for a system with $N = 64$ RIS elements, $K = 4$ transceiver pairs and $L = 70$ pilots.

ing projection algorithm decreases rapidly. This is because the optimization problem (1.20) is highly nonconvex and the alternating projection algorithm starting from different initial points can converge to different solutions, some of which have lower interference power than others. Interestingly, the proposed learning-based approach can make use of the training data to learn a better initial point. From Figure 1.9, we can see that the learning approach can achieve similar performance as the alternating projection algorithm with 30 different random initial points.

1.5. Conclusions

This chapter shows that the RIS can be used not only to adaptively reflect the signals thereby enhancing the direct channels, but also to reduce interference in a multiuser transmission environment. From a theoretical perspective, it can be shown that a rectangular-array RIS is capable of nulling all the interference of a K-user interference channel if the number of RIS elements is sufficiently large when the channels between the RIS and the transceivers are line-of-sight and the direct links can be ignored. From an algorithmic perspective, this chapter presents an alternating projection algorithm that can efficiently find an interference-nulling solution for the general channel models with direct links. Numerically, it is found that the alternating projection algorithm can produce an interference-nulling solution as long as the number of RIS elements is slightly greater than $2K(K-1)$ and the direct links are not too strong. Moreover, for the scenario where CSI needs to be estimated using pilots, unlike the traditional approach of using random initial points for the alternating projection algorithm, the chapter shows that a deep neural network can be trained to learn a better initial point from the estimated CSI. This new approach can result in a much lower interference level at the same number of pilots. In summary, the chapter shows that reducing or nulling interference is a promising use case for RIS in future generation wireless networks.

Bibliography

Andrea Abrardo, Davide Dardari, Marco Di Renzo, and Xuewen Qian. MIMO interference channels assisted by reconfigurable intelligent surfaces: Mutual coupling aware sum-rate optimization based on a mutual impedance channel

model. *IEEE Wireless Commun. Lett.*, 10(12):2624–2628, Dec. 2021. doi: 10.1109/LWC.2021.3109017.

Emil Björnson and Luca Sanguinetti. Rayleigh fading modeling and channel hardening for reconfigurable intelligent surfaces. *IEEE Wireless Commun. Lett.*, 10(4):830–834, Apr. 2021. doi: 10.1109/LWC.2020.3046107.

Tianlong Chen, Xiaohan Chen, Wuyang Chen, Howard Heaton, Jialin Liu, Zhangyang Wang, and Wotao Yin. Learning to optimize: A primer and a benchmark. *Journal of Machine Learning Research*, 23(189):1–59, 2022. URL http://jmlr.org/papers/v23/21-0308.html.

Yali Chen, Bo Ai, Hongliang Zhang, Yong Niu, Lingyang Song, Zhu Han, and H. Vincent Poor. Reconfigurable intelligent surface assisted device-to-device communications. *IEEE Trans. Wireless Commun.*, 20(5):2792–2804, May 2021. doi: 10.1109/TWC.2020.3044302.

Marco Di Renzo, Alessio Zappone, Merouane Debbah, Mohamed-Slim Alouini, Chau Yuen, Julien de Rosny, and Sergei Tretyakov. Smart radio environments empowered by reconfigurable intelligent surfaces: How it works, state of research, and road ahead. *IEEE J. Sel. Areas Commun.*, 38(11):2450 –2525, Nov. 2019. doi: 10.1109/JSAC.2020.3007211.

Min Fu, Yong Zhou, and Yuanming Shi. Reconfigurable intelligent surface for interference alignment in MIMO device-to-device networks. In *IEEE Int. Conf. Commun. (ICC) Workshops*, pages 1–6, Montreal, QC, Canada, June 2021. doi: 10.1109/ICCWorkshops50388.2021.9473762.

Chongwen Huang, Alessio Zappone, George C Alexandropoulos, Mérouane Debbah, and Chau Yuen. Reconfigurable intelligent surfaces for energy effi-

ciency in wireless communication. *IEEE Trans. Wireless Commun.*, 18(8): 4157–4170, Aug. 2019. doi: 10.1109/TWC.2019.2922609.

Zelin Ji, Zhijin Qin, and Clive G. Parini. Reconfigurable intelligent surface aided cellular networks with device-to-device users. *IEEE Trans. Commun.*, 70(3):1808–1819, Mar. 2022. doi: 10.1109/TCOMM.2022.3145570.

Tao Jiang and Wei Yu. Interference nulling using reconfigurable intelligent surface. *IEEE J. Sel. Areas Commun.*, 40(5):1392–1406, May 2022. doi: 10.1109/JSAC.2022.3143220.

Tao Jiang, Hei Victor Cheng, and Wei Yu. Learning to reflect and to beamform for intelligent reflecting surface with implicit channel estimation. *IEEE J. Sel. Areas Commun.*, 39(7):1931–1945, July 2021. doi: 10.1109/JSAC.2021.3078502.

Vishal Monga, Yuelong Li, and Yonina C. Eldar. Algorithm unrolling: Interpretable, efficient deep learning for signal and image processing. *IEEE Signal Process. Mag.*, 38(2):18–44, Mar. 2021. doi: 10.1109/MSP.2020.3016905.

Donald J Newman and André Giroux. Properties on the unit circle of polynomials with unimodular coefficients. *Proc. Amer. Math. Soc.*, 109(1):113–116, 1990. doi: 10.2307/2048369.

Neal Parikh and Stephen Boyd. Proximal algorithms. *Found. Trends Optim.*, 1(3):127–239, 2014. doi: 10.1561/2400000003.

Foad Sohrabi, Tao Jiang, Wei Cui, and Wei Yu. Active sensing for communications by learning. *IEEE J. Sel. Areas Commun.*, 40(6):1780–1794, June 2022. doi: 10.1109/JSAC.2022.3155496.

Qingqing Wu and Rui Zhang. Intelligent reflecting surface enhanced wireless network via joint active and passive beamforming. *IEEE Trans. Wireless Commun.*, 18(11):5394–5409, Nov. 2019. doi: 10.1109/TWC.2019.2936025.

Qingqing Wu, Shuowen Zhang, Beixiong Zheng, Changsheng You, and Rui Zhang. Intelligent reflecting surface-aided wireless communications: A tutorial. *IEEE Trans. Commun.*, 69(5):3313–3351, May 2021. doi: 10.1109/TCOMM.2021.3051897.

Wei Yu, Foad Sohrabi, and Tao Jiang. Role of deep learning in wireless communications. *IEEE BITS the Inf. Theory Mag.*, pages 1–14, early access, 2022. doi: 10.1109/MBITS.2022.3212978.

Zhongze Zhang, Tao Jiang, and Wei Yu. Learning based user scheduling in reconfigurable intelligent surface assisted multiuser downlink. *IEEE J. Sel. Topics Signal Process.*, 16(5):1026–1039, Aug. 2022. doi: 10.1109/JSTSP.2022.3178213.

Özgecan Özdoğan and Emil Björnson. Deep learning-based phase reconfiguration for intelligent reflecting surfaces. In *Asilomar Conf. Signals, Syst., Comput.*, pages 707–711, Pacific Grove, CA, USA, Nov. 2020. doi: 10.1109/IEEECONF51394.2020.9443516.